The FASEB Journal article fj.11-196543. Published online February 13, 2012.

The FASEB Journal • Research Communication

Inhibition of mitochondrial fission prevents cell cycle progression in lung cancer

Jalees Rehman,[*,†] Hannah J. Zhang,[‡] Peter T. Toth,[‡] Yanmin Zhang,[*,†] Glenn Marsboom,[‡] Zhigang Hong,[‡] Ravi Salgia,[§] Aliya N. Husain,[‖] Christian Wietholt,[‡] and Stephen L. Archer[‡,1]

*Section of Cardiology, Department of Medicine, and [†]Department of Pharmacology, University of Illinois at Chicago, Chicago, Illinois, USA; and [‡]Section of Cardiology and [§]Section of Hematology/Oncology, Department of Medicine, and [‖]Department of Pathology, University of Chicago, Chicago, Illinois, USA

ABSTRACT **Mitochondria exist in dynamic networks that undergo fusion and fission. Mitochondrial fusion and fission are mediated by several GTPases in the outer mitochondrial membrane, notably mitofusin-2 (Mfn-2), which promotes fusion, and dynamin-related protein (Drp-1), which promotes fission. We report that human lung cancer cell lines exhibit an imbalance of Drp-1/Mfn-2 expression, which promotes a state of mitochondrial fission. Lung tumor tissue samples from patients demonstrated a similar increase in Drp-1 and decrease in Mfn-2 when compared to adjacent healthy lung. Complementary approaches to restore mitochondrial network formation in lung cancer cells by overexpression of Mfn-2, Drp-1 inhibition, or Drp-1 knockdown resulted in a marked reduction of cancer cell proliferation and an increase in spontaneous apoptosis. The number of cancer cells in S phase decreased from 32.4 ± 0.6 to 6.4 ± 0.3% with Drp-1 inhibition ($P<0.001$). In a xenotransplantation model, Mfn-2 gene therapy or Drp-1 inhibition could regress tumor growth. The tumor volume decreased from 205.6 ± 59 to 70.6 ± 15 mm^3 ($P<0.05$) with Mfn-2 overexpression and from 186.0 ± 19 to 87.0 ± 6 mm^3 ($P<0.01$) with therapeutic Drp-1 inhibition. Impaired fusion and enhanced fission contribute fundamentally to the proliferation/apoptosis imbalance in cancer and constitute promising novel therapeutic targets.—Rehman, J., Zhang, H. J., Toth, P. T., Zhang, Y., Marsboom, G., Hong, Z., Salgia, R., Husain, A. N., Wietholt, C., Archer, S. L. Inhibition of mitochondrial fission prevents cell cycle progression in lung cancer. *FASEB J.* 26, 000–000 (2012). www.fasebj.org**

Key Words: fusion · Drp-1 · mitofusin-2

Cancer cells are characterized by excessive proliferation and increased resistance to apoptosis due to dysregulation of multiple cellular signaling mechanisms (1). Therapeutic approaches that target signaling pathways or metabolic processes preferentially dysregulated in cancer cells are therefore being developed to limit toxicity in nonmalignant cells (2). One such abnormality in cancer is a po_2-independent reliance on glycolysis as the primary source of ATP production (3), but the mechanisms underlying the increase in glycolysis, down-regulation of mitochondrial glucose oxidation, and the ensuing growth/survival advantages for cancer cells are only now being identified (2, 4). Notably, increasing mitochondrial glucose oxidation in cancer cells, using the pyruvate dehydrogenase kinase inhibitor dichloroacetate, slows proliferation and enhances apoptosis in cancer cells and regresses lung cancer in a xenotransplantation model (5). Emerging mitochondria-based cancer therapies primarily focus on the modulation of mitochondrial metabolism (4, 6), but few studies have examined the mitochondrial network structure in cancer.

Mitochondria do not exist as lone organelles, but are part of a dynamic network that continuously undergoes fusion and fission (7). The purpose of fusion and fission is the subject of much speculation and may involve the protection of mitochondrial DNA, altera-

Abbreviations: ^{18}F-FDG, ^{18}F-fluorodeoxyglucose; BrdU, bromodeoxyuridine; Drp-1, dynamin-related protein 1; Fis-1, fission protein 1; hBEC, human bronchial epithelial cell; hPAEC, human pulmonary artery endothelial cell; hPASMC, human pulmonary artery smooth muscle cell; hSAEC, human small airway epithelial cell; mdivi-1, mitochondrial division inhibitor 1; MFC, mitochondrial fragmentation count; Mfn-1, mitofusin-1; Mfn-2, mitofusin-2; micro-CT, micro–computed tomography; mito-PA-GFP, mitochondrial-targeted, photoactivable green fluorescent protein; MNF, mitochondrial networking factor; Opa-1, optic atrophy protein 1; PCNA, proliferating cell nuclear antigen; PET, positron emission tomography; PFU, plaque-forming units; roGFP, redox-sensitive green fluorescent protein; ROS, reactive oxygen species; TMRM, tetramethylrhodamine; TOM20, translocase of outer mitochondrial membrane 20.

[1] Correspondence: Section of Cardiology, University of Chicago, 5841 South Maryland Ave., MC6080, Chicago, IL 60637, USA. E-mail: sarcher@medicine.bsd.uchicago.edu

doi: 10.1096/fj.11-196543

This article includes supplemental data. Please visit *http://www.fasebj.org* to obtain this information.

tion of cellular energetics, and regulation of cell division (7). Multiple mitochondrial membrane GTPases that regulate mitochondrial networking have recently been identified. Mitofusin 1 (Mfn-1) and mitofusin 2 (Mfn-2) initiate fusion by tethering adjacent mitochondria (8), while dynamin-related protein 1 (Drp-1) mediates fission by formation of circumferential, ring-like structures that segment the organelle into discrete fragments (9). Drp-1 is activated by phosphorylation, and a recent study in HeLa cells demonstrated that Drp-1 activation, mediated by a cyclin B1-cdk1-mediated phosphorylation of Drp-1 at Ser-616, and mitochondrial fragmentation occur during mitosis (10). However, little is known about the role of mitochondrial dynamics in cell proliferation and apoptosis in cancer cells. We therefore investigated mitochondrial networking and its potential role as a therapeutic target in human lung adenocarcinoma.

MATERIALS AND METHODS

Cell culture

Human lung cancer cells (A549, H1993, and H358) were purchased from American Type Culture Collection (ATCC; Manassas, VA, USA) and maintained in F12-K (ATCC) or RPMI 1640 (ThermoScientific, Logan, UT, USA) medium supplemented with 10% FBS. Normal human small airway epithelial cells (hSAECs), human bronchial epithelial cells (hBECs), human pulmonary artery smooth muscle cells (hPASMCs), and human pulmonary artery endothelial cells (hPAECs) as well as their culture media were purchased from Lonza (Walkersville, MD, USA). All cells were grown in standard recommended media. Experiments on hSAECs, hBECs, hPASMCs, and hPAECs were performed at passages ≤ 7.

Mitochondrial network imaging

To quantify structural mitochondrial network fragmentation, cells grown in glass-bottom dishes were loaded with mitochondrial red fluorescent dye tetramethylrhodamine (TMRM; 50 nM, 20 min; Molecular Probes, Eugene, OR, USA) in culture medium at 37°C and imaged with the Zeiss 510 META confocal laser scanning microscope using an α Plan-Apochromat ×100/1.46NA objective with ×3 digital zoom (excitation at 561 nm, emission recorded above 575 nm; Carl Zeiss Microimaging, Thornwood, NY, USA). As shown in **Fig. 1*A***, acquired images were background subtracted, filtered (median), thresholded, and binarized to identify mitochondrial segments using ImageJ [U.S. National Institutes of Health (NIH), Bethesda, MD, USA]. Continuous mitochondrial structures were counted with the particle counting subroutine and the number was normalized to the total mitochondrial area (in pixels) to obtain the mitochondrial fragmentation count (MFC) for each imaged cell. For every cell line or intervention, $\geq n = 25$ randomly selected cells were imaged to calculate the respective MFC values.

To quantify functional networking of the mitochondria, we coexpressed a mitochondrial-targeted, photoactivable green fluorescent protein (mito-PA-GFP; ref. 11) and a mitochondrial-targeted DS-Red protein in live cells (12). Expression of mito-DS-Red permits visualization of the complete mitochondrial network, while the mito-PA-GFP enables real-time imaging of individual network components by photoactivation of a discrete region. Imaging experiments were performed 24–96 h following the transfection of the cells using a Zeiss 510 META confocal laser scanning microscope equipped with an

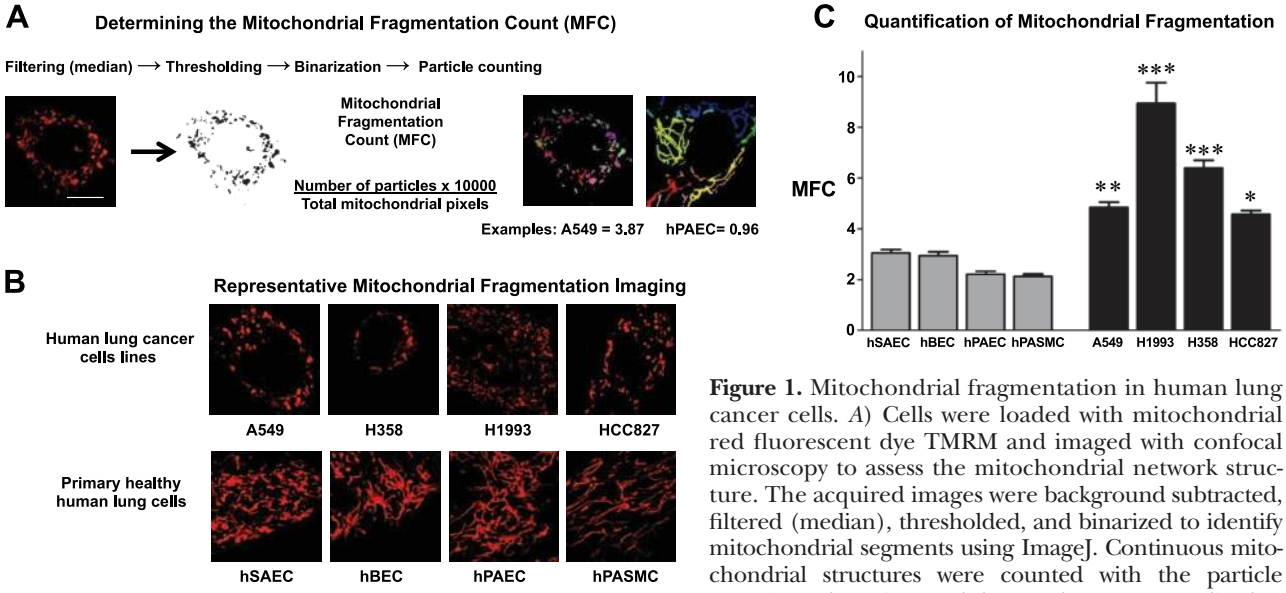

Figure 1. Mitochondrial fragmentation in human lung cancer cells. *A*) Cells were loaded with mitochondrial red fluorescent dye TMRM and imaged with confocal microscopy to assess the mitochondrial network structure. The acquired images were background subtracted, filtered (median), thresholded, and binarized to identify mitochondrial segments using ImageJ. Continuous mitochondrial structures were counted with the particle counting subroutine, and the number was normalized to the total mitochondrial area (in pixels) to obtain the MFC for each imaged cell. For every cell line or intervention, $\geq n = 25$ randomly selected cells were imaged to calculate the respective MFC values. Scale bar = 10 μm (all images). *B*) Representative images of the mitochondrial imaging from cultured human lung cancer cell lines (A549, H358, H1993, HCC827) or human lung epithelial and vascular cells (hSAECs, hBECs, hPAECs, hPASMCs) shows a marked predominance of mitochondrial network fragmentation in the cancer cells. *C*) Quantification of the MFC confirms that all the lung cancer cells lines have a significantly higher level of mitochondrial network fragmentation that any of the nonmalignant human lung epithelial or vascular cells. $^*P < 0.05$, $^{**}P < 0.01$, $^{***}P < 0.001$ *vs.* nonmalignant cells; ANOVA with *post hoc* test.

environmental chamber, to ensure that experiments were conducted at 37°C, at physiological pH, pco_2, and po_2. A ×100 α Plan-Apochromat (1.46NA) objective and ×2 zoom were used to image single cells. Sequential images of fluorescent mitochondria were collected every 17.6 s. Mito-DS-Red was excited at 561 nm, and the emission was recorded using 565-m dichroic and 575-m long-pass filters. Mito-PA-GFP was excited at 488 nm, and the images were acquired at 500–550 nm.

The degree of mitochondrial networking was quantified by defining a mitochondrial networking factor (MNF), which represents the extent of spread of the photoactivated mitochondrial GFP within the mitochondrial network. We measured the area occupied by the photoactivated mitochondrial GFP that diffused away from the site of photoactivation (see **Fig. 2*A***) by quantifying the green fluorescence outside of the photoactivation box in the first image acquired after photoactivation (17.6 s following photoactivation) using ImageJ software. A functionally interconnected network allows the photoactivated GFP to distribute in a larger area. Therefore, a higher MNF signifies greater functional mitochondrial connectivity.

Real-time PCR

Total RNA was isolated from cultured cells or harvested tissues using the PureLink RNA Mini Kit (Invitrogen, Carlsbad, CA, USA) and the total RNA was reverse-transcribed using the High-Capacity cDNA Reverse Transcription Kit (Applied Biosystems, Foster City, CA, USA), following the manufacturer's instructions. The quantitative real-time PCR was performed according to standard protocols. For data analysis, β2 microglobulin (B2M) was used as an endogenous control. Data are expressed as relative expression for each individual gene normalized to their corresponding controls. The primers used were purchased from Applied Biosystems (probe ID: Mfn-1, Hs00966851_m1; Mfn-2, Hs00208382_m1 and Rn00500120_m1; Drp-1, Hs01560976_m1; fission protein 1 (Fis-1), Hs00211420_m1; optic atrophy protein 1 (Opa-1), Hs01047019_m1; translocase of outer mitochondrial membrane 20 (TOM20), Hs00740685-sH; B2M, 4326319E).

Human tissue microarrays

For immunohistochemistry, we studied paraffin-embedded, formalin-fixed tissues from treatment-naive patients with lung adenocarcinoma diagnosed at the University of Chicago Medical Center (Chicago, IL, USA) in accordance with the regulations of the University of Chicago Institutional Review Board, as described previously (13). The tissue cores were arranged on a microscope slide, thus creating a tissue array. This approach ensured that the staining conditions for immunofluorescence were identical between patients and that each tumor sample was matched with normal lung tissue of the same patient. Immunofluorescence assessment of mitochondrial Drp-1 and Mfn-2 expression in human lung sections was performed following antigen retrieval at 95–100°C for 30 min in citrate buffer. The primary antibodies Drp-1 (1:500; Novus Biologicals, Littleton, CO, USA) and Mfn-2 (1:100; Proteintech Group Inc., Chicago, IL, USA) were incubated overnight at 4°C, while secondary antibodies (Alexa Fluor 488, 1:400; and Alexa Fluor 568, 1:400; Invitrogen) were incubated for 1 h at 25°C. DAPI was included in the antifade reagent (Prolong Gold; Invitrogen) for nuclear costaining. Images were acquired with the Zeiss LSM 510 META confocal microscope using the 488- and 561-nm lasers. DAPI was visualized with the Chameleon Ultra (Coherent, Santa Clara, CA, USA) 2-photon laser by setting the wavelength at 770 nm. Nonsaturated Mfn-2 and Drp-1 images were saved as TIFF files, and after background subtraction the nonzero intensity pixel values were averaged using ImageJ.

Immunoblotting for mitochondrial proteins in cell fractions

We used immunoblotting to assess the protein levels of the mitochondrial fission regulator Drp-1 and the phosphorylated forms of Drp-1 (phospho-Drp-1) and to measure mitochondrial release of cytochrome *c*. Fractionation of mitochondrial and cytosolic fractions was performed using the Cell Fractionation kit (MitoSciences, Eugene, OR, USA). For immunoblotting, the following antibodies were used: anti-cytochrome c antibody (1:1000; ab13575; Abcam, Cambridge, MA, USA), anti-Drp-1 antibody (1:1000; NB110-55237; Novus Biologicals), and anti-phospho-Drp1 antibodies (1:1000; Ser-616 and Ser-637; Cell Signaling Technology, Danvers, MA, USA). Immunoblotting was performed using standard protocols. The purity of each fraction was examined by monitoring the level of specific markers with an anti-TOM20 antibody for the mitochondrial fraction (1:500; Santa Cruz Biotechnology, Santa Cruz, CA, USA) and a pan-actin antibody to mark the fraction containing the cytoplasm and cytoskeleton (1:10,000; MAB1501; Millipore, Billerica, MA, USA).

Apoptosis and cell proliferation assays

Apoptosis was assessed by measuring cytochrome *c* release (see preceding section) or by using a standard annexin-based assay kit or a standard TUNEL assay kit (see Supplemental Data for details). Cell proliferation was quantified with a standard bromodeoxyuridine (BrdU) uptake kit (see Supplemental Data).

Molecular modification of mitochondrial networking

A replication-deficient adenovirus containing rat Mfn-2 cDNA was a kind gift from Dr. Kuang-Hueih Chen (NIH, Bethesda, MD, USA). Viruses were amplified and purified by ViraQuest (North Liberty, IA, USA). A virus dose in the range of 1–5 × 10^{10} plaque-forming units (PFU) was used for *in vivo* and *in vitro* experiments. After overnight incubation, the virus was washed out, and cells were harvested 24–48 h after the transfection for the analyses described below. Adenoviruses containing GFP cDNA inserts or without any cDNA inserts were used as vector controls (ViraQuest). The Drp-1 inhibitor, mitochondrial division inhibitor 1 (mdivi-1), was obtained from Enzo Life Sciences (Plymouth Meeting, PA, USA). Mdivi-1 was dissolved in DMSO and added to the culture medium at the designated concentrations. Corresponding amounts of DMSO were used as control treatments.

Mutiple distinct si-RNA and scramble controls to achieve knockdown of Drp-1 were purchased from Integrated DNA Technology (IDT; Coralville, IA, USA). The cells were transfected with the siRNA or scramble controls using either the TriFECTin kit (IDT) or the Lipofectamine RNAiMax kit (Invitrogen) according to the manufacturer instructions. At 72 h after the transfection, knockdown of Drp-1, fragmentation, and apoptosis were assessed.

Assessment of the cellular redox state

The cellular redox state was assessed using a redox-sensitive green fluorescent protein (roGFP) construct (a kind gift from Dr. S. James Remington, University of Oregon), as previously reported (14, 15). Briefly, cells were transfected with the roGFP plasmid with the Fugene HD transfection reagent

(Roche, Basel, Switzerland). By using different excitation wavelengths (400 and 490 nm) and measuring emission at 535 nm, we assessed the redox status of cells. A higher 400/490-nm fluorescence ratio indicates a higher cellular oxidation state. A mitochondrial targeted adenoviral catalase construct (ViraQuest) was used to assess the effect of specifically suppressing mitochondrial H_2O_2 on the cellular redox state.

In vivo xenograft tumor models

Athymic nude mice (5–6 wk old) were obtained from the NIH and housed in the University of Chicago Animal Care Facility. All the animal experiments and procedures conformed to the institutional animal care guidelines. A xenograft model of human lung cancer was established by subcutaneous hindlimb injections of A549 cells ($1–2\times10^6$). When tumors reached ~5 mm diameter (usually 2 wk after xenotransplantation), therapies were initiated. For Ad-Mfn-2 treatment, 1×10^9 PFU (0.1 ml) virus/tumor was injected. For mdivi-1 treatment, 1.75 mg of mdivi-1 in 25 μl of DMSO was injected into each tumor. Equivalent volumes and doses of saline, Ad-GFP, or DMSO were used as control therapies. Tumor size was measured every 4–7 d. At the end of the study (2–3 wk following therapy), animals were sacrificed, and tumors were removed.

Micro–computed tomography (micro-CT) and positron emission tomography (PET) imaging

Mice underwent micro-CT and PET imaging 2–3 wk following therapy. Tumor glucose uptake was quantified by imaging the uptake of ^{18}F-fluorodeoxyglucose (^{18}F-FDG; IBA Molecular, Romeoville, IL, USA; ref 16) using a GE Triumph X-PET preclinical imaging system (GE Healthcare, Piscataway, NJ, USA). To improve the imaging contrast between tumor tissue and normal tissue, mice were unfed for ≥9 h prior to PET imaging (17). Mice were anesthetized using 2% isoflurane immediately before injection of 100 μCi ^{18}F-FDG. Mice were positioned in the imaging system, and temperature and respiratory rate were maintained at 35.7 ± 1.5°C and 55.7 ± 7.6 breaths/min, respectively. Micro-CT data were acquired at 256 positions over a full circle. The CT magnification was set to 1.85, and the total micro-CT imaging time was <2 min. At 30 min after ^{18}F-FDG injection, a 30-min PET acquisition was performed. Micro-CT and PET data were reconstructed using general-purpose filtered backprojection (18) and ordered subset expectation maximization algorithms (19), respectively. Micro-CT data were registered with the PET data sets. Entire tumors were segmented in the reconstructed micro-CT data ,and ^{18}F-FDG tumor uptake was measured in the PET data. ^{18}F-FDG uptake was scaled to correct for variations in animal weight, injected dose, and elapsed time between injection and start of PET data acquisition.

Data analysis

Quantitative data are presented as means ± SE. Statistical analyses were performed using the GraphPad Prism software (GraphPad Inc., La Jolla, CA, USA). Statistical significance of differences between 2 groups was assessed with an unpaired *t* test, while differences between ≥3 groups were assessed by ANOVA with a *post hoc* test or the Kruskal-Wallis test if the value distribution did not meet normality criteria. *In vivo* treatment effects of the mitochondrial fusion therapy on tumor size over time were evaluated with a repeated-measures ANOVA.

RESULTS

Excess mitochondrial fragmentation in lung cancer cells

We compared the degree of mitochondrial network fragmentation in cultured human lung adenocarcinoma cells (A549, H1993, HCC827) and bronchoalveolar carcinoma cells (H358) to that of normal hSAECs, hBECs, hPAECs, and hPASMCs. Representative confocal microscopy images of the mitochondrial networks in each cell type are shown in Fig. 1*B* and demonstrate marked mitochondrial network fragmentation in the all malignant cell types when compared to the control cells. Quantification of the degree of mitochondrial fragmentation using the MFC confirms that the lung cancer cells exhibited a markedly higher degree of structural mitochondrial network fragmentation than control pulmonary cells (Fig. 1*C*).

Excess mitochondrial fission and impaired mitochondrial fusion in cancer cells

We next assessed whether the higher degree of structural mitochondrial network fragmentation resulted in reduced functional mitochondrial connectivity in lung cancer cells. Mito-PA-GFP was used to quantify functional mitochondrial fusion and mitochondrial networking (20). Cells were cotransfected with mito-DS Red (12) to mark the entire mitochondrial network. Fused mitochondria allow focally photoactivated GFP to rapidly transfer along the network. Therefore, the extent of green fluorescence dispersion following photoactivation indicates the degree of functional mitochondrial networking. Mitochondrial networking was quantified using MFN, a new metric we developed, defined as the amount of green signal outside the activation zone at the first image following photoactivation (Fig. 2 *A*). Mitochondria in lung cancer cells had impaired distribution of mito-PA-GFP (low MNF), in marked contrast to the highly networked mitochondria of nonmalignant cells (Fig. 2*B*). Thus, the structural mitochondrial network fragmentation observed in cancer cells (Fig. 1) is associated with an impaired functional connectivity of the mitochondrial matrix.

We then investigated whether reduction in mitochondrial networking in lung cancer cells reflected differences in the expression of some of the key known mediators of mitochondrial fusion or fission using quantitative PCR. As shown in Fig. 2*C*, A549 cells had lower levels of the fusion mediator Mfn-2 and markedly higher levels of the mitochondrial fission mediator Drp-1 than normal airway cells. This finding suggested that the observed mitochondrial fragmentation in A549 cells was related to both impaired fusion and enhanced fission. Other fusion mediators, such as Mfn-1, Opa-1 (21), or Fis-1 (22) were not statistically different between A549 cancer cells and normal hSAECs. Likewise, TOM20, a marker of mitochondrial mass, was similar in A549 cells and hSAECs, suggesting that mitochondrial

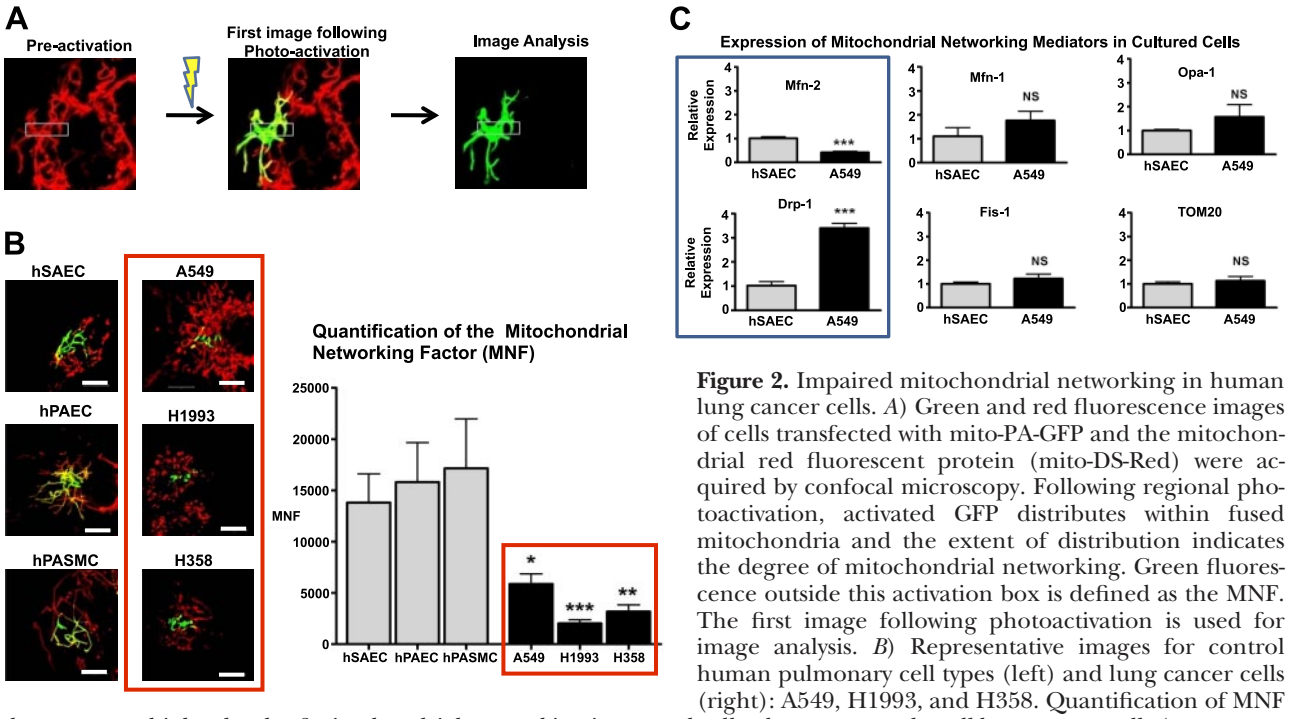

Figure 2. Impaired mitochondrial networking in human lung cancer cells. *A*) Green and red fluorescence images of cells transfected with mito-PA-GFP and the mitochondrial red fluorescent protein (mito-DS-Red) were acquired by confocal microscopy. Following regional photoactivation, activated GFP distributes within fused mitochondria and the extent of distribution indicates the degree of mitochondrial networking. Green fluorescence outside this activation box is defined as the MNF. The first image following photoactivation is used for image analysis. *B*) Representative images for control human pulmonary cell types (left) and lung cancer cells (right): A549, H1993, and H358. Quantification of MNF demonstrates higher levels of mitochondrial networking in control cells when compared to all lung cancer cells (means±SE, $n \geq 6$). *$P < 0.05$, **$P < 0.01$, ***$P < 0.001$. *C*) Quantitative PCR of some key mitochondrial fusion and fission mediators and the mitochondrial mass marker TOM20 in A549 cells and control hSAECs shows a reduction in the expression of Mfn-2 and an increase in Drp-1 in A549 cells (means±SE, $n \geq 3$). NS, not significant. ***$P < 0.001$; *t* test.

fragmentation in lung cancer cells was not due to a generalized loss of mitochondrial mass.

Increased Drp-1 expression and activity in lung cancer

We next examined Mfn-2 and Drp-1 expression in tissue samples from patients with lung adenocarcinoma. Human tissue arrays with lung adenocarcinoma tissue sections and matching sections of adjacent normal lung were used to assess differences in human tissue Drp-1 and Mfn-2 expression. As in the cultured A549 cells, these adenocarcinoma sections had reduced Mfn-2 and increased Drp-1 protein expression when compared to adjacent non-neoplastic lung tissue (**Fig. 3*A***). Quantification of Mfn-2, Drp-1, and proliferating cell nuclear antigen (PCNA) expression in the patient tissue arrays revealed lower levels of Mfn-2 expression and higher levels of Drp-1 in the lung tumor tissue (n=5; Fig. 3*B* and Supplemental Fig. S1). However, a notable diversity was apparent in regional Mfn-2 expression between lung cancer samples from distinct patients as well as heterogeneity within a given tumor. In this latter regard, costaining with PCNA demonstrated that the proliferating tumor cells had lower expression of Mfn-2 than $PCNA^-$ portions of the tumor (Supplemental Fig. S1). We then performed immunoblot analysis to assess the expression of Mfn-2 and Drp-1 expression in cultured lung cancer cells. As shown in the representative immunoblot in Fig. 3*C*, Drp-1 levels were markedly higher and Mfn-2 levels were lower in all lung cancer cell lines except for the HCC827 cell line.

Since the activity of Drp-1, the primary regulator of mitochondrial fission, is regulated by phosphorylation, we also studied its phosphorylation at Ser-616, which enhances Drp-1 activity, and the phosphorylation at Ser-637, which inhibits Drp-1 activity (23). When compared to control epithelial cells, both lung adenocarcinoma cell lines were characterized by increased phosphorylation of Ser-616 and reduced inhibitory phosphorylation of Ser-637 (Fig. 3*D*). Taken together, these findings suggest that lung cancer cells not only manifest higher levels of Drp-1 expression but that the highly expressed Drp-1 is preferentially found in its activated form.

Restoration of mitochondrial networking in A549 cancer cells

To understand the significance of the impaired mitochondrial networking in cancer cells, we studied whether mitochondrial networking in cancer cells could be restored using multiple complementary strategies. We first assessed whether structural mitochondrial fragmentation in cancer cells could be reversed by either using siRNA-mediated knockdown of the fission mediator Drp-1, inhibition of Drp-1 with the highly specific small molecule Drp-1 inhibitor mdivi-1 (24, 25), or overexpression of Mfn-2. All 3 interventions markedly reduced the mitochondrial fragmentation, as shown in the representative images and by quantification of the MFC (**Fig. 4*A***).

To assess whether these interventions also restored functional mitochondrial connectivity, we used the

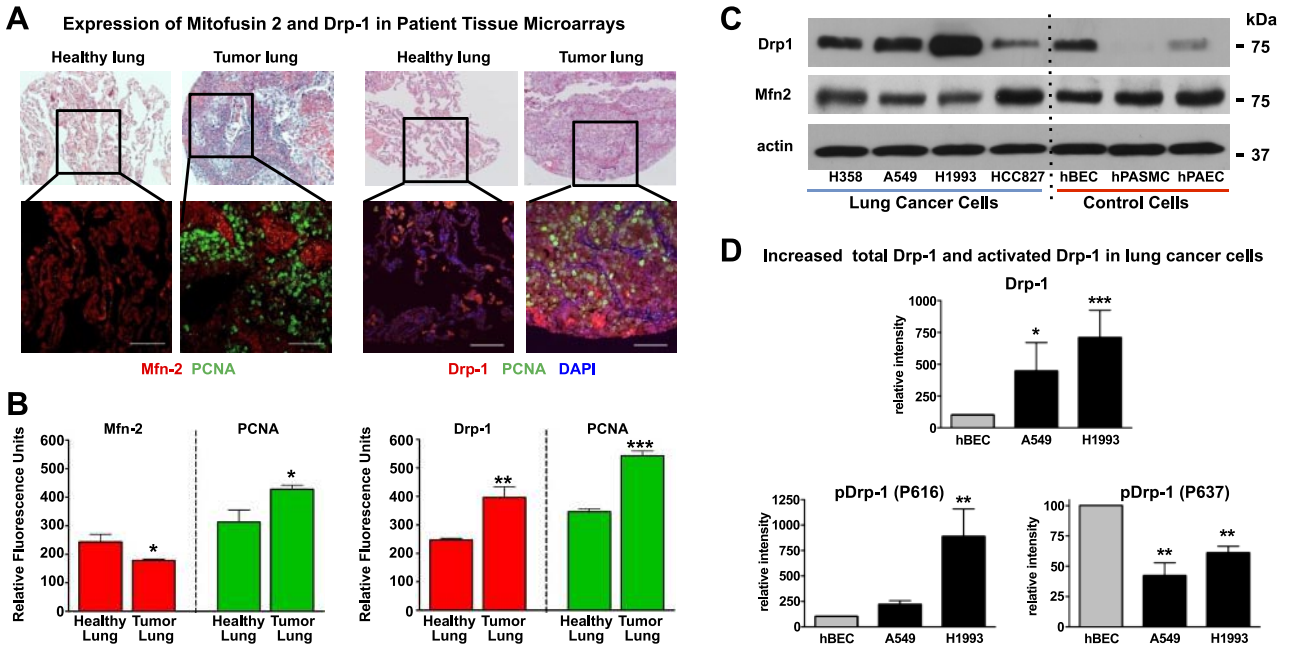

Figure 3. Decreased Mfn-2 and increased Drp-1 in human lung cancer tissue and evidence of Drp-1 activation in lung cancer cells. *A*) Hematoxylin-eosin and immunofluorescence staining in representative human lung and adjacent adenocarcinoma samples. Scale bars = 100 μm. Left panels are stained for Mfn-2 (red) and the proliferation marker PCNA (green). Right panels are stained for Drp-1 (red), the proliferation marker PCNA (green) and the nuclear stain DAPI (blue). *B*) Quantification of immunofluorescence staining (n=5 patients) in relative fluorescence units (RFU, y axis) demonstrates lower levels of Mfn-2 and markedly higher levels of Drp-1 in human lung adenocarcinoma samples (means±SE, t test). NS, not significant. $^*P < 0.05$, $^{**}P < 0.01$, $^{***}P < 0.001$). *C*) Representative immunoblot to assess Drp-1 and Mfn-2 expression in multiple cancer cell lines and control cell lines. Separate gels were run for Drp-1 and Mfn-2 immunoblot analysis, due to their proximity in size and to avoid artifacts related to stripping membranes. Only one representative actin loading control is shown, but actin loading of all lanes was similar on the Mfn-2 and Drp-1 gels. *D*) Immunoblot analysis of Drp-1 phosphorylation was determined with phospho-specific antibodies directed against either phospho-Ser-616 (enhances Drp-1 activity) or phospho-Ser-637 (suppresses Drp-1 activity) in healthy epithelial cells (hBECs) and two distinct human lung adenocarcinoma cell lines (A549 and H1993). Mean intensity for each mitochondrial protein (n≥3, mean intensity normalized to hBEC levels) was quantified and statistical analysis was performed comparing each cancer cell line to hBECs (mean±SE, n≥5). $^*P < 0.05$, $^{**}P < 0.01$, $^{***}P < 0.001$ *vs.* hBECs.

mito-PA-GFP and observed marked increases in the MNF. Figure 4*B* shows representative confocal microscopy time-lapse images of human lung adenocarcinoma cells treated with the control vehicle (top panels), Ad-Mfn2 (middle panels, 24 h post-transfection) or mdivi-1 (bottom panels, 4–6 h after mdivi-1 treatment). Quantification of the MNF showed a 4- to 5-fold increase of functional mitochondrial networking with either therapy (Fig. 4*B*, right panel). Thus, in lung cancer cells, augmentation of Mfn-2 and inhibition or knockdown of Drp-1 yield concordant results, namely, increased mitochondrial networking.

Mfn-2 gene therapy promotes apoptosis and reduces proliferation in lung cancer cells

Cancer cells are characterized by a baseline resistance to apoptosis. Release of mitochondrial cytochrome *c* into the cytosol is a key step in the initiation of the mitochondrial apoptosis pathway (26). Immunoblot assessment of cytochrome *c* in distinct cellular compartments demonstrated a marked increase of cytosolic cytochrome *c* and a decrease of mitochondrial cytochrome *c* when A549 cells were transfected with Ad-Mfn-2 for 24 h *vs.* an adenoviral control vector (**Fig. 5*A***). We further confirmed the induction of apoptosis in A549 cells using TUNEL staining as an indicator of late-stage apoptosis. Compared to control-transfected A549 cells, transfection with Ad-Mfn-2 markedly increased spontaneous TUNEL staining (Fig. 5*B*). In addition to assessing the effects of Mfn-2 overexpression on apoptosis, its effects on A549 cell proliferation was determined using a BrdU uptake assay. There was a marked, dose-dependent decrease in A549 cell proliferation with Mfn-2 overexpression when compared to the overexpression of a control adenoviral vector (Fig. 5*C*).

Because mitochondrial reactive oxygen species (ROS) are a key mediator of cellular apoptosis, we evaluated the cellular redox state using a cytosolic redox-sensitive, green fluorescent protein (roGFP) construct (14). Mfn-2 overexpression markedly increases the cellular oxidation state, which was mitigated by coexpression of mitochondrial-targeted catalase (Fig. 5*D*). This finding suggested that the observed increase in cellular oxidation following

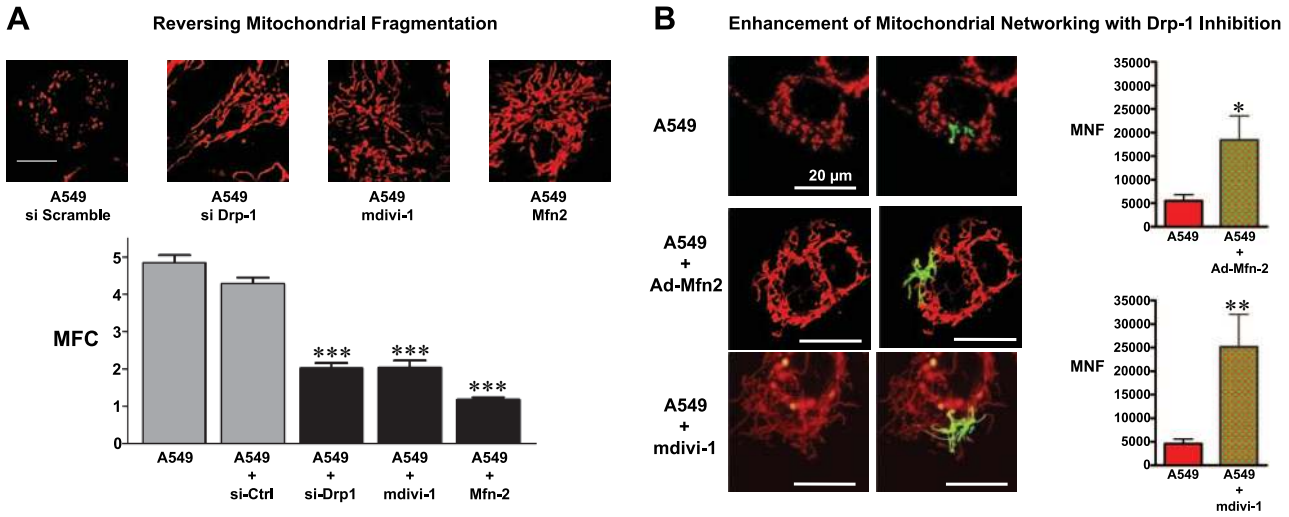

Figure 4. Restoration of mitochondrial networking in A549 cancer cells. *A*) Reversal of the mitochondrial fragmentation in cancer cells was achieved by either using siRNA mediated knockdown of the fission mediator Drp-1 or inhibition of Drp-1 with mdivi-1 or by overexpression of Mfn-2. Images are representative of A549 cells undergoing these interventions or the scramble siRNA control transfection. Scale bar = 10 μm. All 3 interventions achieve a marked reduction in the MFC. ***$P < 0.001$ *vs.* control A549 or scramble siRNA-transfected A549 cells; ANOVA with *post hoc* test. *B*) Confocal microscopy time-lapse images of human lung adenocarcinoma cells expressing the mitochondrial-targeted fluorescent proteins mito-DS-Red (red) and photoactivable GFP (green). Representative confocal microscopy time-lapse images of human lung adenocarcinoma cells treated with the control vehicle (top panels), Ad-Mfn-2 (middle panels, 24 h post-transfection), or mdivi-1, an inhibitor of the mitochondrial fission mediator (bottom panels, 4–6 h following 30 μM mdivi-1 treatment). Quantification of the MNF (*y* axis) shows marked increases in the MNF (means±SE, $n \geq 6$). *$P < 0.05$, **$P < 0.01$; *t* test.

Mfn-2 overexpression reflects increased mitochondrial-derived ROS.

Inhibiting mitochondrial fission increases apoptosis and reduces proliferation in A549 cancer cells

The effects of Drp-1 inhibition as a complementary strategy to augment mitochondrial networking were also assessed. Evaluation of apoptosis by annexin V and PI staining demonstrated that treatment with mdivi-1 for 24 h increased apoptosis (**Fig. 6*A***). Since reports have documented both proapoptotic and antiapoptotic effects of Drp-1 inhibition (24, 25, 27), we conducted a time-course experiment to evaluate whether the proapoptotic effects of Drp-1 inhibition required a threshold duration of continuous mdivi-1 therapy. Significant apoptosis in A549 cells was only observed following a minimum of 16 h of continuous mdivi-1 therapy (Fig. 6*B*). To ensure that proapoptotic effects of mdivi-1 therapy were due to inhibition of Drp-1, we conducted a knockdown of Drp-1 using targeted si-RNA in A549 cells. Knockdown of Drp-1 increased the apoptosis rate 3- to 4-fold in A549 cells, as judged by TUNEL staining (Fig. 6*C*), similar to what we had observed with pharmacological Drp-1 inhibition with mdivi-1. Mdivi-1 also markedly reduced the proliferation of A549 cells, as shown in the representative flow cytometry dot plots in Fig. 6*D*. Flow cytometric quantification revealed that the number of A549 cells in S phase decreased from 32.4 ± 0.6 to 6.4 ± 0.3% with mdivi-1 ($P<0.001$, Fig. 6*E*), proliferation rates similar to those in normal hSAECs. The decreased number of S-phase cells was accompanied by a marked rise in the percentage of A549 cells arrested in G2, suggesting that mdivi-1 prevented completion of the mitotic program. We further investigated this by synchronizing the A549 cells using the cell cycle inhibitor nocodazole, which induced the expected G2 arrest (Supplemental Fig. S2*A*). When cells were released from nocodazole treatment, nearly 80% of the cells moved into the G1 state. However, when cells were maintained in nocodazole or when nocodazole was replaced with mdivi-1, the majority of cells remained in the G2/M phase (Supplemental Fig. S2*B*). This indicated that Drp-1 inhibition with mdivi-1 mimicked the effects of the known cell cycle inhibitor and chemotherapeutic agent nocodazole.

Enhanced mitochondrial networking induces mitochondrial depolarization

A key feature of mitochondrial apoptosis is the collapse of the mitochondrial membrane potential. We therefore evaluated the mitochondrial membrane potential using the potentiometric dye JC-1 and we found a significant loss of mitochondrial membrane potential (depolarization) in A549 cells treated with Mfn-2 overexpression or mdivi-1 (Supplemental Fig. S3). Pharmacologic enhancement of mitochondrial networking with mdivi-1 allowed us to perform a time-course evaluation of this depolarizing effect. Our data show that while mdivi-1 induces mitochondrial networking within 4–6 h (Fig. 4*B*), mitochondrial depolarization begins after 6 h of treatment with mdivi-1 (Supplemental Fig. S3*B*). Interestingly, both therapeutic strategies (Mfn-2

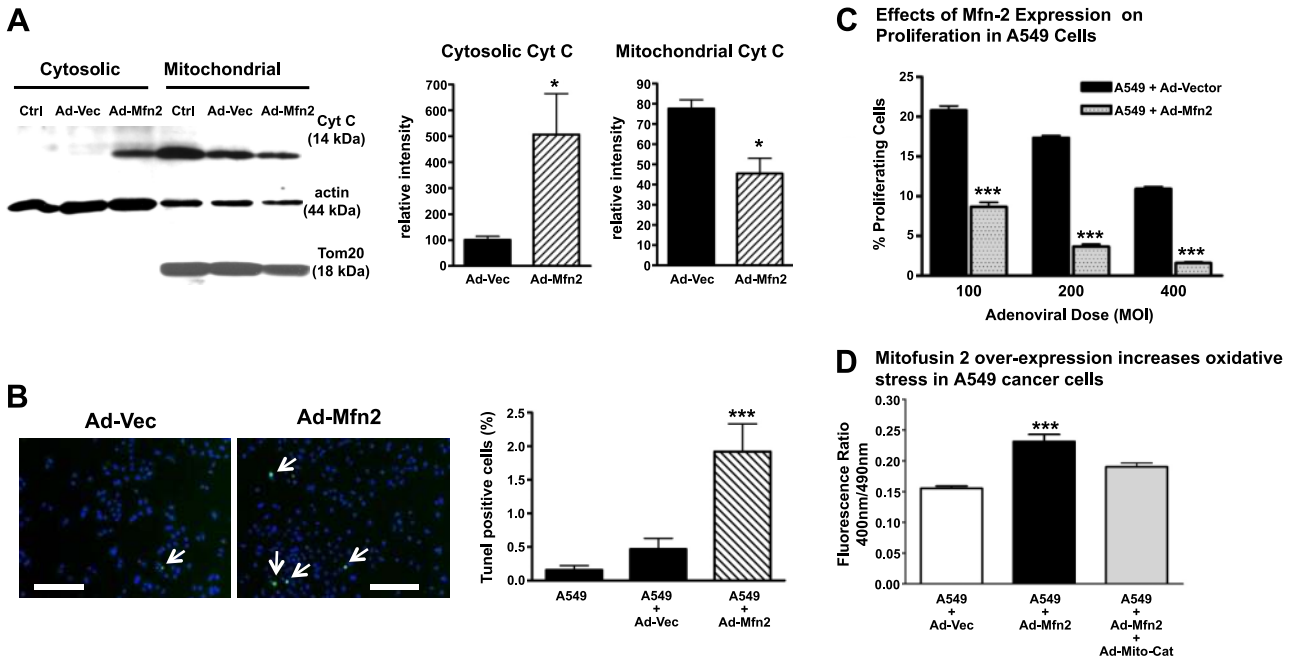

Figure 5. Mfn-2 gene therapy promotes apoptosis and suppresses proliferation in A549 cancer cells. *A*) Compartment-specific immunoblot analysis was performed to analyze the mitochondrial and cytosolic distribution of cytochrome *c*. Left panel: representative immunoblot demonstrates that Ad-Mfn-2 therapy induces mitochondrial apoptosis, as evidenced by redistribution of mitochondrial cytochrome *c* to the cytosolic fraction, when compared to untreated A549 cells (Ctrl) or A549 cells treated with an adenoviral control vector (Ad-Vec). Right panel: quantification of the normalized mean intensity for cytochrome *c* in mitochondrial and cytosolic compartments (means±SE, $n=4$). $^*P < 0.05$; *t* test. *B*) Induction of spontaneous apoptosis with Ad-Mfn-2 transfection in A549 cells was assessed using TUNEL staining. Left panel: representative immunofluorescence images show an increase in TUNEL-positive cells (arrows) with Ad-Mfn-2. Scale bars = 200 μm. Right panel: quantification confirms a marked increase in the percentage of TUNEL-positive cells (means±SE, $n=15$). $^{***}P < 0.001$ *vs.* other treatments. *C*) Proliferation of A549 cells was determined by flow cytometric assessment of BrdU incorporation at 24 h following the transfection. Quantification demonstrates a dose-dependent effect of Ad-Mfn-2 (varying MOI on *x* axis) on the inhibition of cancer cell proliferation when compared to control transfected cells at 24h post-transfection (mean±SE percentage of BrdU-positive cells on *y* axis, $n=3$). $^{***}P < 0.001$; *t* test. *D*) Cellular redox state was assessed using a roGFP construct. The *y* axis of the bar graph shows the redox ratio of cells treated with a control adenoviral vector, with adenoviral Mfn-2, or with the combination of adenoviral Mfn-2 and mitochondrial-targeted catalase. A higher redox ratio indicates a higher oxidation state (means±SE, $n\geq5$). $^{***}P < 0.001$.

overexpression and mdivi-1 treatment) increased cellular ATP levels in A549 cancer cells (Supplemental Fig. S3*C*). This finding suggested that the observed induction of cancer cell apoptosis and decrease in cell proliferation with enhanced mitochondrial networking was not a consequence of ATP depletion.

Enhancing mitochondrial network formation suppresses tumor growth *in vivo*

We then tested the *in vivo* effect of mitochondrial networking therapy on tumor growth using a lung adenocarcinoma xenograft model. At 2 wk following the injection of A549 cells into the hind limbs of immune-deficient, nude mice, tumors (diameter 5–10 mm) were injected with either a Mfn-2-encoding adenovirus or mdivi-1. Control tumors were injected with the same dose of a control adenoviral vector or the mdivi-1 solvent DMSO, respectively. Mice were observed for an additional 2–3 wk following therapy and then underwent micro-CT imaging to evaluate the tumor volume. There was a substantial decrease in tumor size following treatment with either Ad-Mfn-2 or mdivi-1 (**Fig. 7*A***). Representative examples of excised tumors are shown in Fig. 7*B*. Micro-CT, performed 3 wk post-therapy, confirmed a significant reduction in tumor volume with Ad-Mfn-2 or mdivi-1 (Fig. 7*C*). The tumor volume decreased from 205.6 ± 59 to 70.6 ± 15 mm^3 (control vector *vs.* Ad-Mfn-2, $P<0.05$) with Ad-Mfn-2 treatment and from 186.0 ± 19 to 87.0 ± 6 mm^3 (vehicle *vs.* mdivi-1, $P<0.01$) with therapeutic Drp-1 inhibition.

Effect of enhancing mitochondrial network formation on the ^{18}F-FDG uptake of tumors

Cancer cell metabolism is characterized by a shift toward glycolysis that is manifest by increased rates of glucose uptake, which can be measured noninvasively using PET imaging of ^{18}F-FDG uptake. We therefore assessed the ^{18}F-FDG uptake by PET imaging in the tumors that underwent treatment with either Ad-Mfn-2 or mdivi-1. As shown in the representative images in Fig. 7*D*, the total tumor ^{18}F-FDG uptake was reduced by

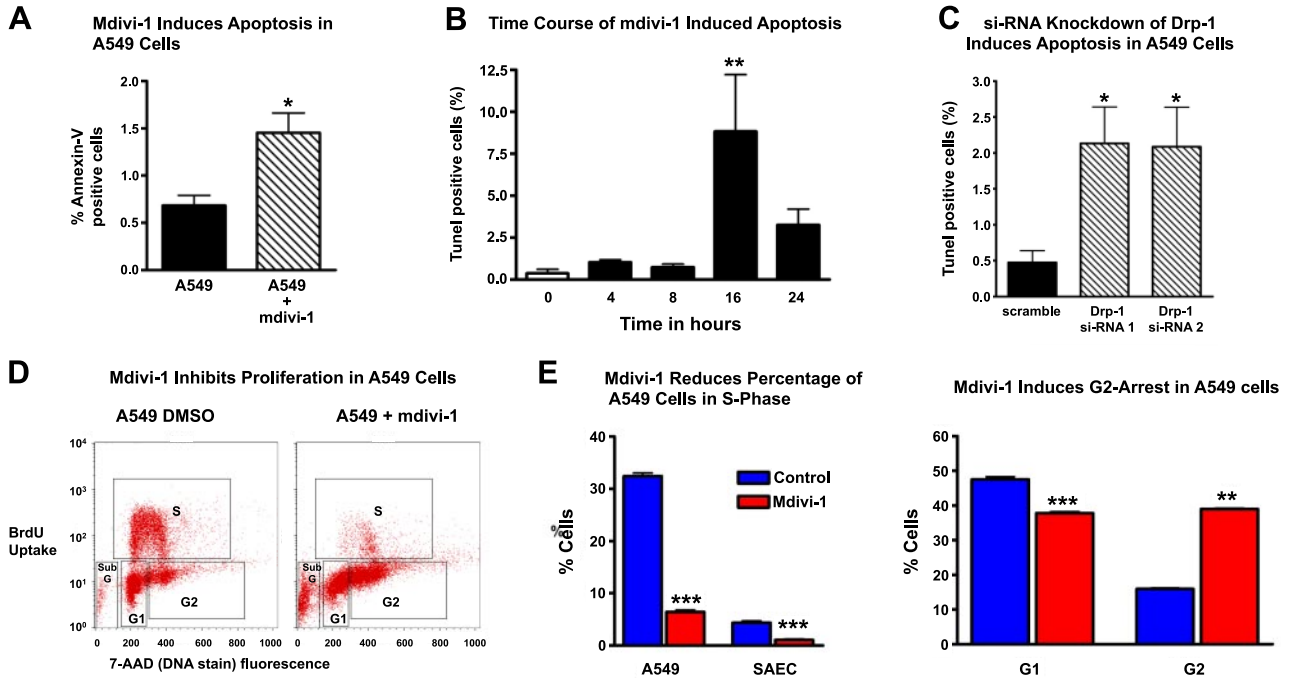

Figure 6. Inhibition of mitochondrial fission with mdivi-1 increases apoptosis and reduces proliferation in A549 cancer cells. *A*) Flow cytometric assessment of apoptosis by annexin V staining in A549 cells treated with either DMSO or the Drp-1 inhibitor mdivi-1 (30 μM for 24 h) showed a significant increase in the percentage of annexin V^+/PI^- cells (*y* axis) with mdivi-1 therapy (means±SE, $n=3$). $^*P < 0.05$; *t* test. *B*) Time course analysis of apoptosis, quantified by TUNEL staining, showed that induction of apoptosis required 16 h of treatment with mdivi-1 (means±SE, $n \geq 10$ at each time point). $^{**}P < 0.01$ *vs.* 0 h; ANOVA with *post hoc* testing. *C*) TUNEL staining was performed on A549 cells undergoing si-RNA knockdown of Drp-1. Percentage of TUNEL-positive cells markedly increased with knockdown of Drp-1 in A549 cells (means±SE, $n \geq 10$). $^*P < 0.05$ *vs.* scramble; ANOVA with *post hoc* analysis. *D*) Flow cytometric cell cycle analysis was performed using BrdU uptake as a marker of cell proliferation (S phase) and the DNA stain 7-AAD. *E*) Mdivi-1(24 h, 30 μM) markedly reduces the percentage of proliferating cells in S phase and concomitantly increases the percentage of cells in G2 phase (meas±SE, $n=3$) $^{**}P < 0.01$, $^{***}P < 0.001$; *t* test.

either therapy. However, when the ^{18}F-FDG uptake was normalized to the tumor volume (Fig. 7*D*), we found no reduction in tumor ^{18}F-FDG uptake per unit tumor volume. Indeed, in the case of mdivi-1, the residual tumor had an even higher ^{18}F-FDG uptake per unit tumor volume, thus suggesting a high level of glucose uptake and glycolysis in the smaller residual tumors.

DISCUSSION

Our data identify 2 distinct and complementary abnormalities that may cause disruption of the mitochondrial network in lung adenocarcinoma cells: impaired fusion and enhanced fission. The fragmented phenotype in multiple lung adenocarcinoma cell lines was associated with down-regulation of the mitochondrial fusion mediator Mfn-2 as well as increased expression of the mitochondrial fission regulator Drp-1. Our study identified high levels of activating Ser-616 Drp-1 phosphorylation and lower levels of inhibitory Ser-637 Drp-1 phosphorylation, thus markedly favoring the active form of Drp-1 in lung cancer cells. Moreover, the identification of a profission signature in lung adenocarcinoma samples from treatment-naive patients (*i.e.*, reduced Mfn-2 and high levels of Drp-1) highlights the translational relevance of our findings. While similar increases in Drp-1 expression that we observed in human lung cancer tissues were also recently reported by another group (28), our study demonstrated that mitochondrial network formation can be restored in lung cancer cells; this in turn reduces cancer cell proliferation and increases apoptosis. Notably, restoring mitochondrial networking also reduced tumor progression *in vivo*.

One emerging strategy to treat cancer targets mitochondrial metabolism, which takes advantage of their dependence on glycolysis as their primary ATP source (the basis for the detection of cancers using FDG-PET scans; refs. 2–5). Interestingly, our PET imaging data did not show any significant decrease in the glucose uptake of the residual tumor following enhancement of the mitochondrial networking. Our findings therefore suggest a novel paradigm for mitochondrial-targeted cancer therapy, namely targeting mitochondrial networking. This could form the basis of a complementary approach to cancer therapy, which may be additive to or synergize with therapies that limit cancer cell proliferation by enhancing mitochondrial glucose oxidation.

It has been shown previously that Mfn-2 overexpression can limit cell proliferation in vascular cells (29) or cancer cells (30). Our experiments demonstrate that

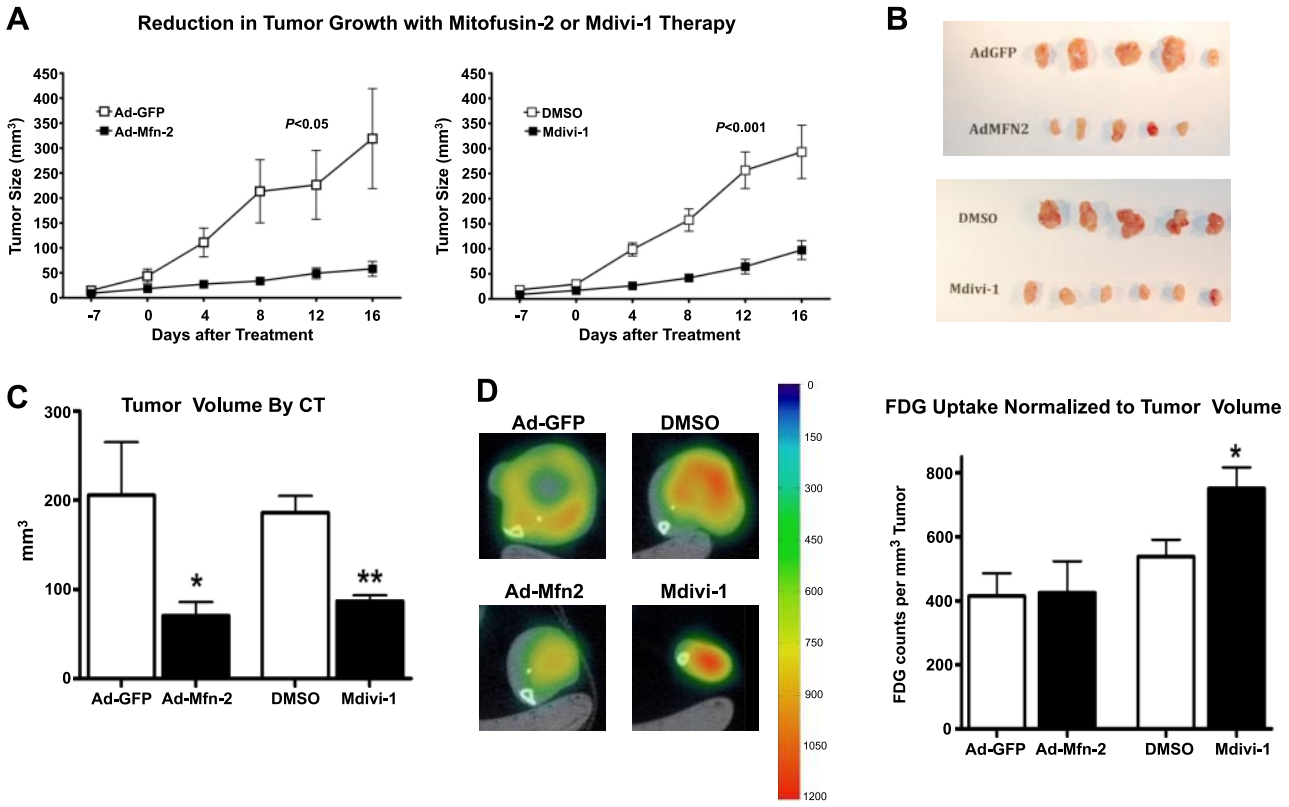

Figure 7. Enhancing mitochondrial network formation suppresses tumor growth *in vivo*. *A*) Tumor size assessed over time in nude mice is shown as calculated volume (mm^3; means±SE, n=9/group). Therapeutic interventions were applied 2 wk after tumor implantation (d 0). Ad-Mfn-2 and mdivi-1 both prevented tumor progression ($P<0.05$ *vs.* control Ad-GFP and $P<0.01$ *vs.* control DMSO, respectively, by repeated measures ANOVA). *B*) Representative excised tumors from animals that were treated either with control therapies (Ad-GFP or DMSO) or the fusogenic therapies (Ad-Mfn-2, mdivi-1). *C*) Tumor volume (mm^3 on y axis, n=9/group) was measured radiographically by micro-CT 2–3 wk post-therapy and demonstrated a significant decrease in tumor volume with Ad-Mfn-2 therapy or mdivi-1 treatment. $^*P < 0.05$, $^{**}P < 0.01$; t test. *D*) ^{18}F-FDG uptake in implanted xenograft tumors was measured by PET; representative scans are shown for the respective treatment groups, and a color scale is attached to indicate the glucose uptake. Quantification of ^{18}F-FDG uptake (^{18}F-FDG counts/mm^3, y axis) was normalized to tumor volume. No significant effect was found with Ad-Mfn-2 therapy on ^{18}F-FDG uptake of the residual tumor, but an increase was found in ^{18}F-FDG uptake of residual tumors in mdivi-1-treated tumors (means±SE, n=9/group) $^*P < 0.05$; t test.

both Mfn-2 and mdivi-1 therapies increase mitochondrial network formation. Mdivi-1, which increases mitochondrial networking by inhibiting Drp-1, achieved similar suppression of proliferation as did the Mfn-2 overexpression. These observations support the interpretation that the forced increase in mitochondrial networking in cancer cells can contribute to a decrease in cancer cell proliferation. The observed increase in oxidative stress and mitochondrial depolarization suggest that enhanced mitochondrial networking may induce cell cycle arrest or spontaneous apoptosis in cancer cells *via* modulation of mitochondrial ROS. However, additional studies are necessary to investigate the specific mechanisms by which enhanced mitochondrial networking may affect mitochondrial depolarization and ROS levels and the downstream targets.

The fact that Drp-1 inhibition suppresses proliferation in cancer cells is especially intriguing, because prior studies in nonmalignant cells have found discordant results regarding how Drp-1 activity affects cell survival and proliferation. One study by Szabadkai *et al.* (27) demonstrated that Drp-1 overexpression can prevent apoptosis, while other studies have found that inhibition of Drp-1 by mdivi-1 can prevent cell death and promote cell proliferation (24, 31). However, it is important to note that these latter studies used short-term exposure of cells to mdivi-1 (≤4 h) to achieve a prosurvival or proliferative effect. Mitra *et al.* (31) showed that short-term exposure to mdivi-1 increased the buildup of cyclin E in normal rat kidney cells and facilitated their entry into the S phase of the cell cycle. Conversely, the researchers found that prolonged treatment with mdivi-1 resulted in the chronic presence of hyperfused mitochondria and chronic elevation of cyclin E, which prevented the progression of the cell cycle (31). Our studies indicate that mdivi-1 treatment of A549 cells for 24 h also resulted in a marked reduction of cells in S phase and an increase of cells in G2 arrest. Future studies will be necessary to investigate how the hyperfused mitochondrial reticulum affects the progression of the cell cycle. Whether mitochondrial fusion or inhibition of mitochondrial fission can result in increased survival and growth or increased apoptosis is very likely contextual, since mitochondrial fission is a

key mediator for 2 very distinct processes: cellular apoptosis (25) and cell mitosis (10).

Our study focused on the role of Mfn-2 and Drp-1 in cancer cell proliferation; however, it is likely that additional mediators and regulators of mitotic mitochondrial fission may also play a key role in cancer cell proliferation. Recent studies have demonstrated that mitochondrial elongation factor 1 (MIEF-1) and mitochondrial fission factor (MFF) can affect Drp-1 localization and activity and thus regulate mitochondrial fission (32, 33). Another recent study has identified the small Ras-like GTPase RALA as a key regulator of Drp-1 phosphorylation and activation during mitotic mitochondrial fission in human HEK cells (34). Considering the fact that Ras-like GTPases such as RALA are thought to drive oncogenic transformation and tumor progression in cancer (35), future studies could address the role of Ras-like GTPase dysregulation of mitotic mitochondrial fission as well as the role of the newly identified MIEF1 and MFF proteins in cancer cells.

During recent years, the expanding field of mitochondrial network biology has drawn much interest, as it is becoming clear that the network state has a significant effect on cell survival and function. Our study has identified mitochondrial fission and Drp-1 activation as a novel therapeutic target in lung cancer. Future studies are necessary to investigate mitochondrial fusion and fission in other cancers and hyperproliferative diseases and to employ targeted therapies that enhance mitochondrial networking based on the underlying molecular abnormalities of mitochondrial fusion and fission, which likely varies among tumor types. FJ

This work is supported in part by the Harold Hines Jr. Chair in Medicine and U.S. National Institutes of Health (NIH) grants NIH-RO1-HL071115 (S.A.), 1RC1HL099462-01 (S.A), NIH-K08-HL080082 (J.R.), NIH-R01-GM094220 (J.R.), NIH-R01-CA125541-04 (R.S.), and NIH-R01-CA 129501-02 (R.S.). The authors thank the following colleagues for providing the tools to study mitochondrial networking: Dr. Richard Youle (NIH, Bethesda, MD, USA) for the mito-PA-GFP plasmid, Dr. Michael Frohman (Stony Brook University, Stony Brook, NY, USA) for the mito-DS-Red plasmid, Dr. S. James Remington (University of Oregon, Eugene, OR, USA) for the redox-sensitive ro-GFP plasmid, Dr. Kuang-Hueih Chen (NIH) for the adenovirus containing rat mitofusin-2 cDNA, and Dr. Frederick E. (Rick) Domann, Jr. and Dr. Shawn Flanagan (University of Iowa, Iowa City, IA, USA) for the adenovirus containing the cDNA of human mitochondrially targeted catalase.

REFERENCES

1. Evan, G. I., and Vousden, K. H. (2001) Proliferation, cell cycle and apoptosis in cancer. *Nature* **411,** 342–348
2. Deberardinis, R. J., Sayed, N., Ditsworth, D., and Thompson, C. B. (2008) Brick by brick: metabolism and tumor cell growth. *Curr. Opin. Genet. Dev.* **18,** 54–61
3. Hsu, P. P., and Sabatini, D. M. (2008) Cancer cell metabolism: Warburg and beyond. *Cell* **134,** 703–707
4. Gogvadze, V., Orrenius, S., and Zhivotovsky, B. (2009) Mitochondria as targets for chemotherapy. *Apoptosis* **14,** 624–640
5. Bonnet, S., Archer, S. L., Allalunis-Turner, J., Haromy, A., Beaulieu, C., Thompson, R., Lee, C. T., Lopaschuk, G. D., Puttagunta, L., Bonnet, S., Harry, G., Hashimoto, K., Porter, C. J., Andrade, M. A., Thebaud, B., and Michelakis, E. D. (2007) A mitochondria-K+ channel axis is suppressed in cancer and its normalization promotes apoptosis and inhibits cancer growth. *Cancer Cell* **11,** 37–51
6. Gao, P., Tchernyshyov, I., Chang, T. C., Lee, Y. S., Kita, K., Ochi, T., Zeller, K. I., De Marzo, A. M., Van Eyk, J. E., Mendell, J. T., and Dang, C. V. (2009) c-Myc suppression of miR-23a/b enhances mitochondrial glutaminase expression and glutamine metabolism. *Nature* **458,** 762–765
7. Detmer, S. A., and Chan, D. C. (2007) Functions and dysfunctions of mitochondrial dynamics. *Nat. Rev. Mol. Cell Biol.* **8,** 870–879
8. Koshiba, T., Detmer, S. A., Kaiser, J. T., Chen, H., McCaffery, J. M., and Chan, D. C. (2004) Structural basis of mitochondrial tethering by mitofusin complexes. *Science* **305,** 858–862
9. Frank, S., Gaume, B., Bergmann-Leitner, E. S., Leitner, W. W., Robert, E. G., Catez, F., Smith, C. L., and Youle, R. J. (2001) The role of dynamin-related protein 1, a mediator of mitochondrial fission, in apoptosis. *Dev. Cell* **1,** 515–525
10. Taguchi, N., Ishihara, N., Jofuku, A., Oka, T., and Mihara, K. (2007) Mitotic phosphorylation of dynamin-related GTPase Drp1 participates in mitochondrial fission. *J. Biol. Chem.* **282,** 11521–11529
11. Karbowski, M., Lee, Y. J., Gaume, B., Jeong, S. Y., Frank, S., Nechushtan, A., Santel, A., Fuller, M., Smith, C. L., and Youle, R. J. (2002) Spatial and temporal association of Bax with mitochondrial fission sites, Drp1 and Mfn2 during apoptosis. *J. Cell Biol.* **159,** 931–938
12. Choi, S. Y., Huang, P., Jenkins, G. M., Chan, D. C., Schiller, J., and Frohman, M. A. (2006) A common lipid links Mfn-mediated mitochondrial fusion and SNARE-regulated exocytosis. *Nat. Cell Biol.* **8,** 1255–1262
13. Ma, P. C., Jagadeeswaran, R., Jagadeesh, S., Tretiakova, M. S., Nallasura, V., Fox, E. A., Hansen, M., Schaefer, E., Naoki, K., Lader, A., Richards, W., Sugarbaker, D., Husain, A. N., Christensen, J. G., and Salgia, R. (2005) Functional expression and mutations of c-Met and its therapeutic inhibition with SU11274 and small interfering RNA in non-small cell lung cancer. *Cancer Res.* **65,** 1479–1488
14. Hanson, G. T., Aggeler, R., Oglesbee, D., Cannon, M., Capaldi, R. A., Tsien, R. Y., and Remington, S. J. (2004) Investigating mitochondrial redox potential with redox-sensitive green fluorescent protein indicators. *J. Biol. Chem.* **279,** 13044–13053
15. Archer, S. L., Marsboom, G., Kim, G. H., Zhang, H. J., Toth, P. T., Svensson, E. C., Dyck, J. R., Gomberg-Maitland, M., Thebaud, B., Husain, A. N., Cipriani, N., and Rehman, J. (2010) Epigenetic attenuation of mitochondrial superoxide dismutase 2 in pulmonary arterial hypertension: a basis for excessive cell proliferation and a new therapeutic target. *Circulation* **121,** 2661–2671
16. Ong, L. C., Jin, Y., Song, I. C., Yu, S., Zhang, K., and Chow, P. K. (2008) 2-[18F]-2-deoxy-D-glucose (FDG) uptake in human tumor cells is related to the expression of GLUT-1 and hexokinase II. *Acta Radiol.* **49,** 1145–1153
17. Fueger, B. J., Czernin, J., Hildebrandt, I., Tran, C., Halpern, B. S., Stout, D., Phelps, M. E., and Weber, W. A. (2006) Impact of animal handling on the results of 18F-FDG PET studies in mice. *J. Nucl. Med.* **47,** 999–1006
18. Pan, X., Xia, D., Zou, Y., and Yu, L. (2004) A unified analysis of FBP-based algorithms in helical cone-beam and circular cone- and fan-beam scans. *Phys. Med. Biol.* **49,** 4349–4369
19. Hudson, H. M., and Larkin, R. S. (1994) Accelerated image reconstruction using ordered subsets of projection data. *IEEE Trans. Med. Imaging* **13,** 601–609
20. Karbowski, M., Norris, K. L., Cleland, M. M., Jeong, S. Y., and Youle, R. J. (2006) Role of Bax and Bak in mitochondrial morphogenesis. *Nature* **443,** 658–662
21. Frezza, C., Cipolat, S., Martins de Brito, O., Micaroni, M., Beznoussenko, G. V., Rudka, T., Bartoli, D., Polishuck, R. S., Danial, N. N., De Strooper, B., and Scorrano, L. (2006) OPA1 controls apoptotic cristae remodeling independently from mitochondrial fusion. *Cell* **126,** 177–189

22. Lee, Y. J., Jeong, S. Y., Karbowski, M., Smith, C. L., and Youle, R. J. (2004) Roles of the mammalian mitochondrial fission and fusion mediators Fis1, Drp1, and Opa1 in apoptosis. *Mol. Biol. Cell* **15,** 5001–5011
23. Chang, C. R., and Blackstone, C. (2010) Dynamic regulation of mitochondrial fission through modification of the dynamin-related protein Drp1. *Ann. N. Y. Acad. Sci.* **1201,** 34–39
24. Cassidy-Stone, A., Chipuk, J. E., Ingerman, E., Song, C., Yoo, C., Kuwana, T., Kurth, M. J., Shaw, J. T., Hinshaw, J. E., Green, D. R., and Nunnari, J. (2008) Chemical inhibition of the mitochondrial division dynamin reveals its role in Bax/Bak-dependent mitochondrial outer membrane permeabilization. *Dev. Cell* **14,** 193–204
25. Brooks, C., Wei, Q., Cho, S. G., and Dong, Z. (2009) Regulation of mitochondrial dynamics in acute kidney injury in cell culture and rodent models. *J. Clin. Invest.* **119,** 1275–1285
26. Brenner, D., and Mak, T. W. (2009) Mitochondrial cell death effectors. *Curr. Opin. Cell Biol.* **21,** 871–877
27. Szabadkai, G., Simoni, A. M., Chami, M., Wieckowski, M. R., Youle, R. J., and Rizzuto, R. (2004) Drp-1-dependent division of the mitochondrial network blocks intraorganellar Ca2+ waves and protects against Ca2+-mediated apoptosis. *Mol. Cell* **16,** 59–68
28. Chiang, Y. Y., Chen, S. L., Hsiao, Y. T., Huang, C. H., Lin, T. Y., Chiang, I. P., Hsu, W. H., and Chow, K. C. (2009) Nuclear expression of dynamin-related protein 1 in lung adenocarcinomas. *Mod. Pathol.* **22,** 1139–1150
29. Chen, K. H., Guo, X., Ma, D., Guo, Y., Li, Q., Yang, D., Li, P., Qiu, X., Wen, S., Xiao, R. P., and Tang, J. (2004) Dysregulation of HSG triggers vascular proliferative disorders. *Nat. Cell Biol.* **6,** 872–883
30. Wu, L., Li, Z., Zhang, Y., Zhang, P., Zhu, X., Huang, J., Ma, T., Lu, T., Song, Q., Li, Q., Guo, Y., Tang, J., Ma, D., Chen, K. H., and Qiu, X. (2008) Adenovirus-expressed human hyperplasia suppressor gene induces apoptosis in cancer cells. *Mol. Cancer Ther.* **7,** 222–232
31. Mitra, K., Wunder, C., Roysam, B., Lin, G., and Lippincott-Schwartz, J. (2009) A hyperfused mitochondrial state achieved at G1-S regulates cyclin E buildup and entry into S phase. *Proc. Natl. Acad. Sci. U. S. A.* **106,** 11960–11965
32. Zhao, J., Liu, T., Jin, S., Wang, X., Qu, M., Uhlen, P., Tomilin, N., Shupliakov, O., Lendahl, U., and Nister, M. (2011) Human MIEF1 recruits Drp1 to mitochondrial outer membranes and promotes mitochondrial fusion rather than fission. *EMBO J.* **30,** 2762–2778
33. Otera, H., Wang, C., Cleland, M. M., Setoguchi, K., Yokota, S., Youle, R. J., and Mihara, K. (2010) Mff is an essential factor for mitochondrial recruitment of Drp1 during mitochondrial fission in mammalian cells. *J. Cell Biol.* **191,** 1141–1158
34. Kashatus, D. F., Lim, K. H., Brady, D. C., Pershing, N. L., Cox, A. D., and Counter, C. M. (2011) RALA and RALBP1 regulate mitochondrial fission at mitosis. *Nat. Cell Biol.* **13,** 1108–1115
35. Bodemann, B. O., and White, M. A. (2008) Ral GTPases and cancer: linchpin support of the tumorigenic platform. *Nat. Rev. Cancer* **8,** 133–140

Received for publication September 23, 2011.
Accepted for publication January 30, 2012.